PAPER

A bio-inspired looming detection for stable landing in unmanned aerial vehicles*

IOP Publishing Bioinspir. Biomim. 20 (2025) 016007 https://doi.org/10.1088/1748-3190/ad8d99

Bioinspiration & Biomimetics

PAPER

RECEIVED
18 June 2024

REVISED
20 October 2024

ACCEPTED FOR PUBLICATION
25 October 2024

PUBLISHED
13 November 2024

A bio-inspired looming detection for stable landing in unmanned aerial vehicles*

Yupeng Xie, Zhiteng Li, Linkun Song and Jiannan Zhao**

Guangxi Key Laboratory of Intelligent Control and Maintenance of Power Equipment, School of Electrical Engineering, Guangxi University, Nanning 530004, People's Republic of China

**Author to whom any correspondence should be addressed.

E-mail: cqu_zjn@hotmail.com

Keywords: micro aerial vehicles, stable landing, looming cues, monocular vision

Abstract

Flying insects, such as flies and bees, have evolved the capability to rely solely on visual cues for smooth and secure landings on various surfaces. In the process of carrying out tasks, micro unmanned aerial vehicles (UAVs) may encounter various emergencies, and it is necessary to land safely in complex and unpredictable ground environments, especially when altitude information is not accurately obtained, which undoubtedly poses a significant challenge. Our study draws on the remarkable response mechanism of the Lobula Giant Movement Detector to looming scenarios to develop a novel UAV landing strategy. The proposed strategy does not require distance estimation, making it particularly suitable for payload-constrained micro aerial vehicles. Through a series of experiments, this strategy has proven to effectively achieve stable and high-performance landings in unknown and complex environments using only a monocular camera. Furthermore, a novel mechanism to trigger the final landing phase has been introduced, further ensuring the safe and stable touchdown of the drone.

1. Introduction

Unmanned aerial vehicles (UAVs) have been widely utilized in various fields, such as military reconnaissance, geological surveys, and the inspection of power lines [1, 2]. In these applications, UAVs are frequently tasked with autonomously executing flight missions within complex or perilous environments. Achieving a safe and efficient landing under complex and uncertain terrain conditions emerges as a critical challenge among these tasks. In the case of larger UAVs, the incorporation of laser rangefinders has facilitated secure and effective landings [3]. Nonetheless, this approach may not be viable for smaller UAVs. With the ongoing trend towards the miniaturization of electronic products [4], the physical dimensions of flying robots are similarly diminishing. This progression not only calls for a reduction in the weight of onboard components but also emphasizes maximizing functionality while striving to minimize size to the greatest extent feasible. The onboard camera is entrusted with video recording and environmental sensing as the pivotal visual sensor. In situations of extreme constraints, the ability to employ a solitary onboard camera for both operational and sensory tasks represents a significant design objective and challenge within the realm of micro UAV development.

Notably, flying animals in nature have successfully evolved the capability to address similar challenges, relying solely on vision to freely choose and smoothly land on various substrates. For instance, bees utilize optical flow cues for landing [5, 6], maintaining a constant rate of optical expansion in their field of view. This method results in both approach speed and landing height concurrently approaching zero. As they get closer to the landing surface, bees extend their legs to aid in a safe landing. Bumblebees adopt a similar strategy but periodically switch to new constant rates of optical expansion during the landing process [7], allowing for a faster approach to the surface. Birds, such as pigeons [8], achieve simple landing control through the tau function of the optical variable x, where the tau function is

* This research was funded by the National Natural Science Foundation ofchina, grant number 62206065, and the Bagui Scholar Program of Guangxi.

defined as the ratio of the optical variable x to its rate of change, approximating the time until contact with the landing surface. By maintaining a constant rate of change in the tau function, they control the landing and extend their legs just before contact. Hummingbirds [9] and mallards [10] also demonstrate similar tau function landing mechanisms.

The ingenious landing mechanisms of flying animals have provided a rich source of inspiration for enhancing the landing technology of micro UAVs [11–13], with particular attention paid to the use of optical flow by flying insects to achieve landing [14]. Optical flow encompasses information on speed and distance, but these elements are coupled, making them difficult to decouple. Floris van Breugel [15] introduced a method called dynamic peering to achieve landing utilizing optical flow cues, which also allows for the estimation of the UAV's speed and distance during the landing process. However, this method encounters significant estimation errors during the initial phase of landing and can result in oscillations during the final approach to landing. Researchers like Guido de Croon *et al* [16, 17]. have developed a stability-based strategy that uses optical flow manipulation and control inputs for monocular distance estimation. There is a linear relationship between the oscillations of the UAV at different heights and the controller gain, that is, the oscillations at different heights corresponds to different controller gains. The gain is known and the oscillation can be detected, and this strategy estimates distance by detecting self-induced oscillations as the surface approaches, enhancing the UAV's distance estimation capabilities under wind influence and throughout the landing process. Tests on the Parrot AR Drone 2.0 demonstrated its effectiveness during hovering and landing phases. However, while outlining the relationship between control gains and altitude, this method did not improve the performance of optical flow control. In existing research, an adaptive gain control strategy [18] is proposed for optical flow-based landing to deal with the fundamental gain selection problem. After setting an appropriate initial gain, it is incrementally increased until the UAV experiences oscillation, followed by a descent where the gain is exponentially decreased to achieve a high-performance landing. This method avoids oscillations as the UAV approaches the landing surface. However, increasing the gain is required to induce initial oscillations, consuming time and delaying immediate landing. Another study [19] explores a landing approach based on supervised learning, which enables flying robots to learn from visual appearances to estimate distances. This method allows for distance perception without inducing oscillations in the UAV. However, implementing self-supervised learning on autonomous robots adds complexity, as the robot's own movements can influence the dataset. Unlike adjusting gains based on altitude, a landing strategy based on time-to-contact, named TauPilot, has been implemented on rotary-wing UAVs [20]. The idea of this strategy is to gradually reduce the contact time and adjust the gain according to the contact time. However, this strategy needs to give a suitable initial gain according to the altitude and speed, and an inappropriate initial gain will seriously affect the performance of the subsequent landing.

Previous research has successfully applied bio-inspired strategies to achieve autonomous and stable landings in flying robots, highlighting the value of drawing inspiration from nature. Estimating landing distance is a viable landing strategy. However, literature [21] suggests that insects may complete their landing maneuvers without relying on speed and distance, relying solely on optical cues, which evidently conserves more energy for small flying insects. The diverging optical flow contain information on both velocity and altitude, but it is vulnerable to optic flow caused by lateral movement, making it difficult to select information on the main direction of flight. On the other hand, biological studies have shown that the characteristics of looming motion contain information about the speed of its own motion and the distance from the object [22]. This feature is proportional to the speed of the movement and implicitly contains distance information, which can be used to control behavior in various contexts, including the control of landing behavior. Looming motion can be understood as the motion of an oncoming object. In landing case, the looming motion is the dominant motion. Furthermore, a neuron involved in landing control is present in *Drosophila* [23, 24], which is thought to encode visual looming features and control the onset of landing in a behavior-dependent manner. Biological findings suggests landing rely on looming cues is effective, let along, unlike diverging optic flow, looming sensitive algorithm will naturally filter the interfere optic information unrelated to oncoming motion, which means it will be robust to lateral movement or disturbance during landing. However, landing strategy based on looming cues has yet to be implemented in UAV.

In this study, we propose a smooth landing strategy based on looming cues. We employ the Distributed Synaptic Connection LGMD (D-LGMD) model [25], inspired by locust neurons, to detect looming cues during the landing phase. This model enhances the detection of approaching movements while minimizing irrelevant motion. We extract looming motion information in the entire visual field and use fuzzy control techniques to achieve an autonomous landing. The proposed method relies on visual information without requirement on high-resolution. This means our architecture is available for those vertical landing UAVs (e.g. quadrotors) with regular downward camera. It does not require

conventional distance gauging instruments like laser rangefinders and radars and prerequisites such as depth estimation from visual imagery. Excellent performance is achieved in complex simulated outdoor environments, such as grass or between urban buildings. We have also proposed a mechanism to trigger the final landing phase, enabling the UAV to deploy its landing gear at the appropriate time, similar to how a bee extends its legs before touching down on a surface.

2. Principles and methods

The intensity of optical flow and looming motion information both increase as they approach the ground. Optical flow captures information from all types of motion within the field of view. In addition to forward motion, drones often experience uncontrolled lateral movements during landing, which leads to interfere to the visual algorithm. The looming detection algorithm selected in this paper is inspired by the locust giant movement detector (LGMD) neuron, which is inherently insensitive to translational motion [25]. Therefore, it can effectively utilize looming motion information during the landing process. We propose a landing strategy based on looming cues (The landing flowchart of the model is shown in figure 1), which uses techniques such as looming detection and fuzzy control to achieve a smooth landing of the UAV. The algorithm demonstrates strong generalization capabilities and computational efficiency. It exhibits a high degree of distinction between looming and non-looming information, which also leads to a highly nonlinear response. Consequently, the algorithm's output response exhibits some degree of discontinuity. To address this characteristic, we designed a discrete fuzzy controller to reduce the impact of this discontinuity on landing performance. In this section, we will introduce the design process of the looming detection model and the controller, respectively.

2.1. Looming cues detected

Our model leverages the LGMD to identify looming cues in the landing phase [26, 27]. Situated in the locust's brain, LGMD neurons are specialized visual neurons designed to detect motion, showing a pronounced preference for the rapid expansion indicative of an object coming closer. The bio-inspired model for these neurons was initially developed by Rind and Bramwell in 1996 [28] and has subsequently been enhanced and refined by researchers including Blanchard *et al* [29], Yue *et al* [30], Stafford *et al* [31], and Silva *et al* [32]. It has found applications in collision detection systems for terrestrial vehicles [33] and aerial drones [25]. In our research, we employ the D-LGMD model, as proposed by Zhao *et al* [25], to discern looming movements during descent. This

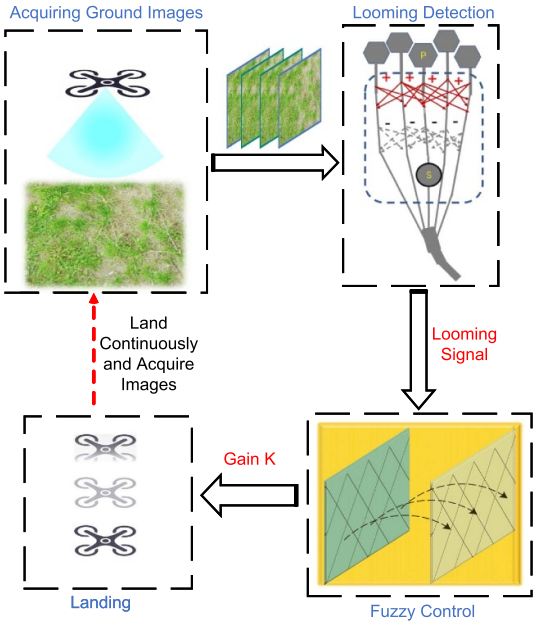

Figure 1. This diagram shows the approximate process of landing. Acquiring Ground Images: This is acquired through the camera at the bottom of the drone. Looming Detection: The image is processed to obtain an looming signal. Fuzzy Control: The speed gain factor is obtained by analyzing the looming signal. Landing: The landing speed of the UAV is adjusted by the speed gain factor.

adaptation of the model increases its ability to selectively respond to looming movements while minimizing the response to less relevant visual motion patterns. A detailed exposition of the D-LGMD model's architecture and its underlying mathematical framework follows(The framework is shown in figure 2).

Photoreceptor Layer (*P*-Layer): The first layer of the D-LGMD model consists of photoreceptor cells arranged in parallel. Its primary function is to monitor the absolute luminance changes of each pixel in the input image, extracting motion changes in the field of view. The motion in the image will activate the photoreceptor cells of the *P*-layer, after which the information about the moving edges is transmitted to the subsequent neural network layer. The formula is defined as follows:

$$P_t(x,y) = |I_t(x,y) - I_{t-1}(x,y)|. \quad (1)$$

In equation (1), $I_t(x,y)$ represents the brightness value of pixel (x,y) at time t, and the output $P_t(x,y)$ records the brightness change between two frames at the same position.

The DPC Layer: The DPC layer, by employing distributed presynaptic connections, plays a crucial role in the development of looming selectivity within the D-LGMD model, enhancing the response to stimuli of looming. This layer comprises parallel arrays of excitatory pathways (referred to as the *E*-layer) and inhibitory pathways (referred to as the *I*-layer), along with an *S*-layer. The latter is tasked with linearly

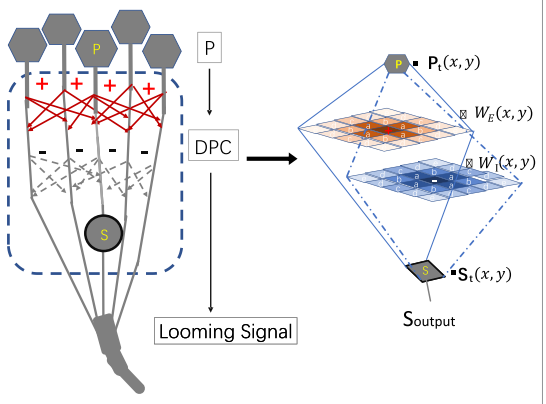

Figure 2. The diagram of D-LGMD model. The left side shows the neuron architecture, and the right side shows the detailed structure of the DPC layer, where the excitatory and inhibitory layers mutually determine the output.

mapping the excitatory and inhibitory information. Motion edge information received from upstream neural networks is processed through both the *E* and *I* layers, which in turn, output excitatory and inhibitory information respectively:

$$E(x,y) = \sum_{i=-N}^{N}\sum_{j=-N}^{N} P_t(x+i,y+j)\cdot W_E(i,j) \quad (2)$$

$$I(x,y) = \sum_{i=-N}^{N}\sum_{j=-N}^{N} P_t(x+i,y+j)\cdot W_I(i,j). \quad (3)$$

Here, W_E and W_I represent the excitatory and inhibitory convolution kernels, respectively, with the excitatory kernel encompassing spatial domain distribution, while the inhibitory kernel features characteristics of both spatial and temporal domain distributions. The size of the convolution kernels is $2N \times 2N$, and both employ Gaussian kernel distributions to describe their spatial extent:

$$W_E(i,j) = G_{\sigma E}(i,j) \quad (4)$$

$$W_I(i,j) = G_{\sigma I}(i,j)\cdot\delta(t-\tau(i,j)). \quad (5)$$

In equations (4) and (5), σE and σI are the standard deviations of the Gaussian distributions of the excitatory and inhibitory kernels, respectively, and $\tau(i,j)$ is the time mapping function of the inhibitory pathway, where the delay time is determined by distance:

$$\tau(i,j) = \alpha + \frac{1}{\beta + e^{-\lambda^2(i^2+j^2)}}. \quad (6)$$

In equation (6), α, β, λ are constants, which play the role of adjusting the time distribution. Then, the information from these two ways is linearly mapped in the *S*-layer:

$$S_t(x,y) = E_t(x,y) - a\cdot I_t(x,y) \quad (7)$$

$$S_t(x,y) = \begin{cases} S_t(x,y) & \text{if } S_t(x,y) \geqslant 0, \\ 0 & \text{if others.} \end{cases} \quad (8)$$

The generation of synaptic stimulation is a result of the linear integration of outputs from both excitatory and inhibitory pathways. In this process, the output from the excitatory pathway, which promotes neural activity, combines with that of the inhibitory pathway, which suppresses it, to determine the final level of synaptic activation. The inhibitory index, represented by *a* in the formula, reflects the intensity of background noise suppression. It's worth noting that the value of synaptic stimulation is constrained to be non-negative, a constraint that is reflected in equation (8), to maintain the stability of the neural network and prevent potential over-inhibition.

Following the aforementioned motion extraction process, the *S*-layer successfully captured the visual information of looming. We have computed the zeroth moment of the *S*-layer's output:

$$S_{\text{output}} = \sum\sum S_t(x,y). \quad (9)$$

This step transforms the characteristics of the looming motion into a specific numerical output, which is the looming signal output by the LGMD perception module. This signal is then used as the input for our controller.

2.2. Design of fuzzy controller

Given the highly nonlinear and non-smooth characteristics typically exhibited by the output of the LGMD algorithm, this study employs a fuzzy controller to accommodate these attributes. Fuzzy control is a control method based on fuzzy logic that is well-suited for handling uncertainty and nonlinear systems. Compared to traditional precise control, fuzzy control uses fuzzy rules and membership functions to simplify complex system dynamics into straightforward control strategies, making it particularly useful in scenarios with complex environments and uncertainties. Fuzzy control, by processing discrete inputs, can generate smoother control outputs, offering precise guidance for the control during the UAV's landing process.

We have developed a single-input, single-output fuzzy logic controller (as shown in figure 3). This controller receives the output from the LGMD perception module as input and generates a gain factor K_n, which acts on the velocity of the previous moment. Consequently, the velocity of the UAV for the next moment is adjusted accordingly(The downward velocity is the positive direction):

$$v_{t+\Delta t} = K_n \cdot v_t \quad (10)$$

where, Δt is the time interval of the speed gain factor, which is used to describe the reaction time of the UAV

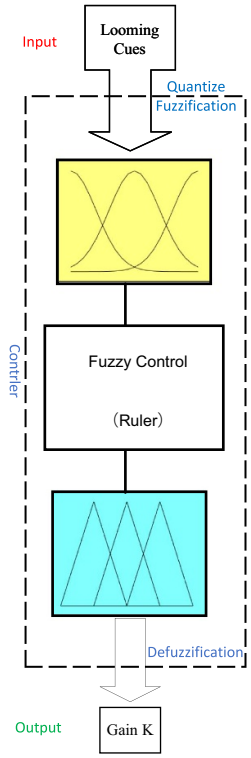

Figure 3. Fuzzy Logic Controller Diagram. The input is looming information, and the output is a velocity gain factor. The dashed box with a yellow background represents the membership functions for the input, where the input variables are fuzzified. The blue background indicates the membership functions for the output, where the defuzzification process occurs. The central block with a white background encapsulates the fuzzy relationships between the input and output variables, forming the core of the controller.

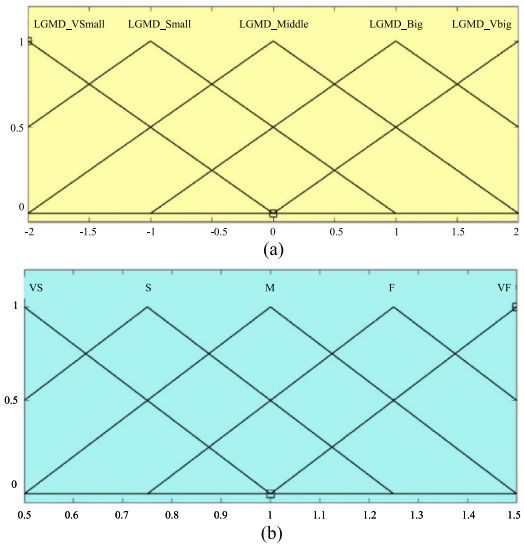

Figure 4. Membership Function Diagram. (a) Membership functions for input variables. (b) Membership functions for output variables.

between the change of speed v_t to $v_{t+\Delta t}$. It reflects the inertia and response delay of the system.

The operation of the fuzzy logic controller can be succinctly divided into three parts: fuzzification, rule-base establishment, and defuzzification. Drawing on expert experience and the characteristics of the LGMD perception module, we designed the input-output membership functions and rule base using the Simulink Fuzzy Logic Toolbox in MATLAB/Simulink, as illustrated in figure 4.

To accommodate the broad span of outputs from the LGMD perception module and simplify the design and tuning process of the membership functions, we quantized the output values into five levels: −2, −1, 0, 1, and 2. This quantization range is adjustable. Subsequently, we defined five fuzzy linguistic variables: LGMD_VSmall (very small), LGMD_Small (small), LGMD_Middle (medium), LGMD_Big (large), and LGMD_VBig (very large), to sequentially describe the scale of outputs from the LGMD perception module. Each fuzzy linguistic variable corresponds to a membership function, which characterizes the degree to which a specific domain value belongs to a fuzzy linguistic variable.

The controller outputs a velocity gain factor to adjust the UAV's next command speed, defined using fuzzy linguistic variables as VS (Very Slow), S (Slow), M (Medium), F (Fast), and VF (Very Fast). The fuzzy sets 'VS' and 'S' imply applying a negative gain to decelerate the UAVs, 'M' maintains the current speed, and 'F' and 'VF' apply a positive gain to increase the landing speed.

Precise definitions of input and output fuzzy linguistic variables and their adjustments enable more accurate control. Establishing a rule base is fundamental for implementing these controls, as the controller relies on this rule base to function. We have established the following five rules:

①	IF Input = LGMD_VBig,	THEN Output = VS.
②	IF Input = LGMD_Big,	THEN Output = S.
③	IF Input = LGMD_Middle,	THEN Output = M.
④	IF Input = LGMD_Small,	THEN Output = F.
⑤	IF Input = LGMD_VSmall,	THEN Output = VF.

When the input fuzzy variable is LGMD_VSmall, indicating that the UAV might be at a higher altitude or experiencing a slower descent rate, it is appropriate to increase the UAV's descent speed, following rule one. If the UAV's descent speed is too fast or it is very close to the ground, deceleration is required to control the landing, as specified by rule five. Rule three applies when the UAV's response to the ground is at a medium level, with an ambiguous landing state, and it is advised to maintain the current speed for landing. Rules two and four act as buffers to prevent significant

control adjustments due to sudden state changes. It is important to note that these rules are not triggered in isolation but are simultaneously active and interact with each other. We focus primarily on the fuzzy variable that most significantly impacts the landing. Therefore, the fuzzy variables are converted into specific speed gain factors by adopting the average maximum membership principle for defuzzification.

3. Experiments and results

We developed a highly detailed simulation environment that closely replicates real-world features using the Unreal Engine 4, focusing on quadcopter drones as the subject of our study. It can provide realistic visual effects and realistic physical simulations, thus reproducing the working scenes of robots in complex environments [34]. And we verified the effectiveness of the algorithm on various landing surfaces. To ensure the rigor of the experiments, environmental conditions such as lighting, temperature, and wind speed are maintained consistently across different landing scenarios.

Before initiating the landing process, the UAV ascends to a designated altitude of 5 meters and awaits the landing command. The bottom of the UAV was equipped with a conventional camera with a 90 ° field of view and a resolution of 500×500 pixels. This parameter was used in the experiments under all scenarios. Once the landing command is issued, the camera captures ground images, triggering the start of the landing procedure. AirSim [35] is an open-source, cross-platform simulation tool based on the Unreal Engine, which provides many interfaces that allow us to interact with simulated environments and drones. Throughout the descent, data on altitude, speed, and acceleration were collected at a frequency of 30 Hz using the AirSim API interface. All experiments were conducted on a desktop computer equipped with an Intel-i5 2.5 GHz CPU and 32GB of memory.

3.1. Landing experiments across various scenarios

In multiple experiments conducted across various scenarios, the landing performance of the UAV is illustrated in figure 5. We selected several representative scenarios for our landing experiments. They were on the indoor ground with the concentric ring logo (The diameter of the outermost ring is about 1 meter), the stone brick pavement, the concrete road and the grass (figure 4 from left to right). We choose to test in these scenarios, because when the UAV needs to land in the field for reconnaissance work or in an emergency situation, it often chooses to land on a relatively flat ground such as grass. If the UAV is flying over a city and needs to land, it is more likely to land on a sidewalk or a non-threatening road surface. It is worth mentioning that we do the landing experiment on the concentric ring sign for two purposes. First, we test the landing effect on simple patterns to prepare for landing in complex scenes. Second, we want to provide some new ideas for guided landing methods that determine the pose of the UAV through ground markers. Whether our method can help the UAV free from the estimation of altitude, and only need to adjust the horizontal position of the UAV to achieve a small error landing. In order to simulate the real flight environment as much as possible, some of these scenes were generated in the simulation environment, such as the heart ring sign, the stone brick road and the concrete road, and the grass scene was the real data input into the simulation.

When initiating the landing sequence from a hover state, our algorithm responds immediately to commence descent. The UAV gradually accelerates, reaching its peak velocity when it is approximately halfway to the landing surface and then enters a deceleration phase. In indoor environments marked with symbols and outdoor grassy areas, the UAV's peak speeds exceed 2 $\mathrm{m\,s^{-1}}$, whereas landing on a stone brick pavement surface sees peak speeds around only 1 $\mathrm{m\,s^{-1}}$. Different landing surfaces present varying threats of looming motion. The line texture of the stone brick road is more dense and complex than that of the other three scenes. At the same height or speed, landing on the stone brick road will perceive a higher threat of looming motion. As a result, the drone triggers deceleration at a higher altitude, which takes more time to land. Following deceleration, the UAV experienced two brief accelerations from the speed curve, which improved the time efficiency of landing on the premise of ensuring safety. In our experiment, we also notice a certain degree of discontinuity in the velocity curve, which we analyze and discuss. Despite some degree of discontinuity in the velocity, it is worth noting that the overall altitude trajectory remains smooth and stable, ensuring the overall performance of the system in the landing mission. For some application scenarios, such discontinuities are acceptable in tasks with high tolerance to some flight accuracy and speed variations. In some more demanding scenarios and tasks, it is necessary to further verify the reliability and applicability of the current method, and further optimize the algorithm to improve the continuity of the speed.

It is noteworthy that we have also proposed a strategy to trigger the final landing phase of the UAV. During the descent, the LGMD signal strength will increase as the UAV approaches the landing surface, and this strategy will be triggered when the signal level remains consistently high. In the LGMD signal curve shown in figure 4, we considered this strategy to be activated when the signal value exceeds the order of 2×10^6 and the duration reaches more than 400 milliseconds. At this point, the UAV can open the landing gear or perform other actions that are conducive to landing. This is similar to insects in nature that

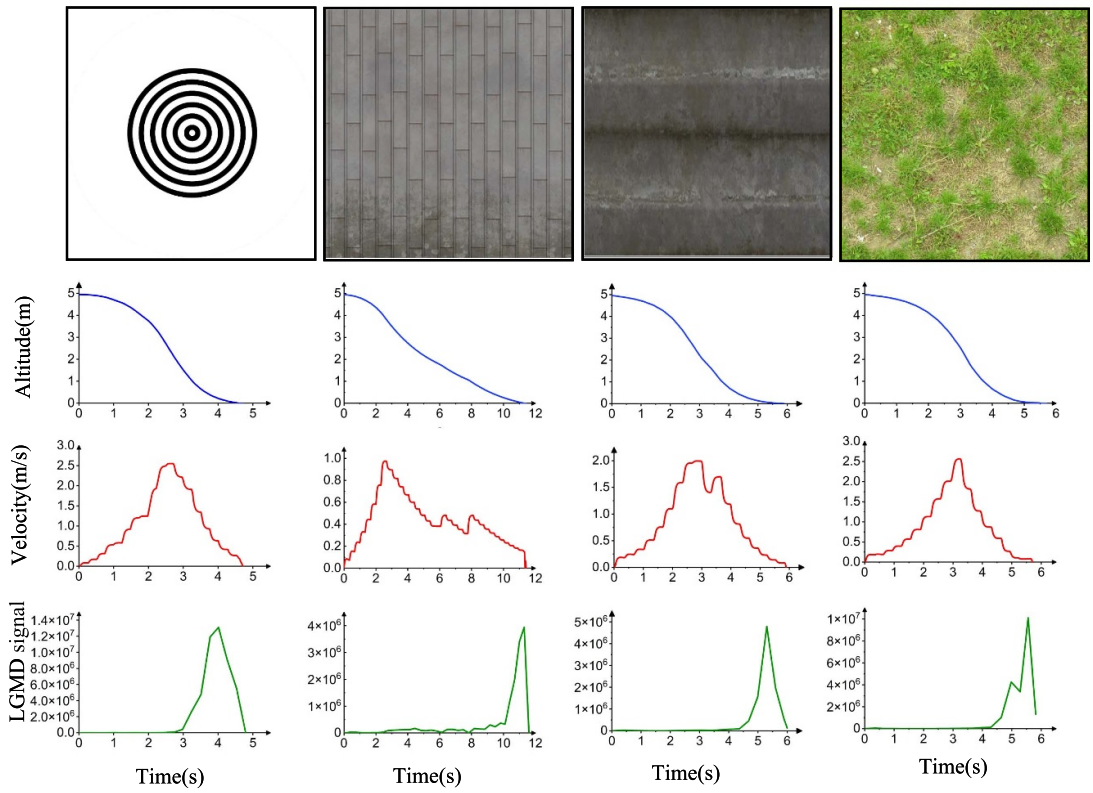

Figure 5. Autonomous landing experiments with the control algorithm were carried out indoors (the ground on which the concentric ring symbols were placed) and outdoors (the stone brick pavement, the concrete road, and the grass, respectively) scenarios, and the curves of altitude (blue), velocity (red), and LGMD looming signals (green) during the landing process as a function of time was recorded in each scenario, respectively.

Table 1. We present statistics on the landing results in various environments, which are averaged over multiple test data (The value in parentheses is the standard deviation of each item). The surfaces are numbered as follows, 1: concentric ring; 2: stone brick pavement; 3: concrete road; 4: grass. Each scenario was tested 10 times.

Surface	Time (s)	Average Velocity ($m\,s^{-1}$)	Trigger Height(m)	Integration of Snap
1	4.9 (0.27)	1.02 (0.064)	0.88 (0.048)	2994.4 (119.5)
2	11.5 (1.03)	0.43 (0.037)	0.14 (0.020)	2226.1 (57.6)
3	5.9 (0.34)	0.85 (0.050)	0.17 (0.029)	2338.8 (55.0)
4	6.0 (0.43)	0.83 (0.059)	0.13 (0.016)	2420.7 (66.9)

extend their legs to attach to the surface of flowers or leaves when they are about to land on the surface of a medium, and we provided a reasonable and practical mechanism for this. From the LGMD signal curve, this strategy can respond about 1 before the UAV reaches the ground, and the lower the preset trigger signal level, the earlier this response is. If the trigger signal is set too high, there is a chance that the policy will not be activated, because in some scenarios the high signal duration is too short to achieve a sustained trigger time. Therefore, it is more reliable to set the trigger value at a low value, even though this may result in activating this strategy when it is far from the ground.

To better understand the applicability and robustness of the algorithm, we conducted some data analysis on the landing results. We collected performance data for landings on various surfaces, including landing time, average speed, altitude at the moment of triggering the final landing mechanism, and the snap integral, which is used as an indirect measure of energy consumption. The results are shown in table 1.

3.2. Experimental comparison and evaluation

In addition to the method proposed in this paper, we conducted comparative experiments to analyze the effectiveness of the strategy for achieving stable landings in unknown environments. The experimental content includes: (1) Utilizing a proportional controller to maintain the looming signal at a certain level during the landing process, termed the constant looming signal strategy, to facilitate the UAV's landing in unknown environments. (2) Comparing

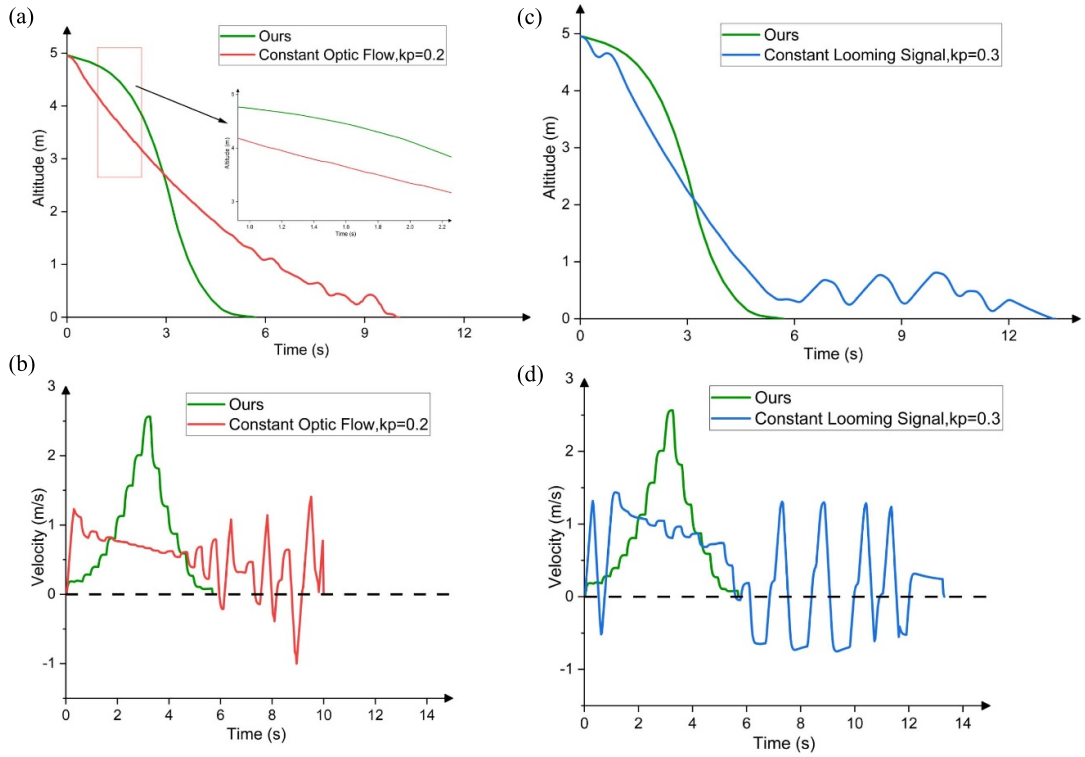

Figure 6. Comparison experiments. (a) and (b) Show the comparison with the constant optical flow strategy. (c) and (d) Are compared with the constant looming signal landing strategy. By zooming in on the image at the 2-second mark in (a), local irregularities in the altitude trajectory can be observed.

the proposed method with the constant optical flow divergence landing strategy.

Under identical external conditions, the aforementioned experiments were conducted, with detailed results presented in figure 6. All experiments would start from the same landing position, which ensures that the UAV did not land on a surface with different characteristics and affected the comparison results. We chose the grass surface shown in figure 5 for the landing experiments of each algorithm, which is the real data input to the simulation scenario. During the landing process, we used the same frame rate (35 frames per s) to collect information such as the height and speed of the UAV, which could ensure that the data is fair when comparing and evaluating. The internal and external parameters of the UAV were unchanged during the experiment. When implementing the constant looming signal landing strategy, the LGMD signal is first normalized. Signals below a magnitude of 10^7 were normalized to a range of 0 to 1, while signals exceeding this threshold were set directly to 1. The normalization is to make the LGMD signal smoother. Subsequently, the landing speed of the UAV was adjusted by the proportional controller to maintain the normalized LGMD signal at 0.3. It can be expressed as: $u = k(s - s_{\text{set}})$, where k is the scaling factor, s is the normalized looming signal input to the controller, s_{set} is the desired normalized LGMD signal, and the controller output u is the throttle of the UAV. The constant optical flow strategy is similar to the constant looming signal strategy. The difference is that the constant optical flow strategy only obtains the optical flow value of a small area of interest (usually a small rectangular area, refer to [15] for details) in the center of the image. During the landing process, the optical flow value of this part of the area is kept unchanged, and the speed and altitude of the UAV naturally converge to zero.

Under the control strategy based on maintaining a constant looming signal, it was observed that the UAV rapidly increased its speed at the beginning of the descent in order to quickly adjust the looming stimulus to a target level close to 0.3. However, as the UAV approached the ground, significant oscillations occurred, leading to increased landing time. This phenomenon is clearly depicted in the experimental images. In contrast, our proposed method initiated the descent at a slower speed but accelerates in the latter half of the landing process, maintaining stability without any oscillations. In the constant optical flow divergence landing strategy, oscillations also occurred when approaching the ground. Our method, however, achieved a stable approach. The optical flow-based method falls faster in the beginning. When the optical flow strategy starts to fall, the optical flow in the visual field will be quickly adjusted to the desired value, so the fall speed will increase rapidly. However, in this process, the landing trajectory

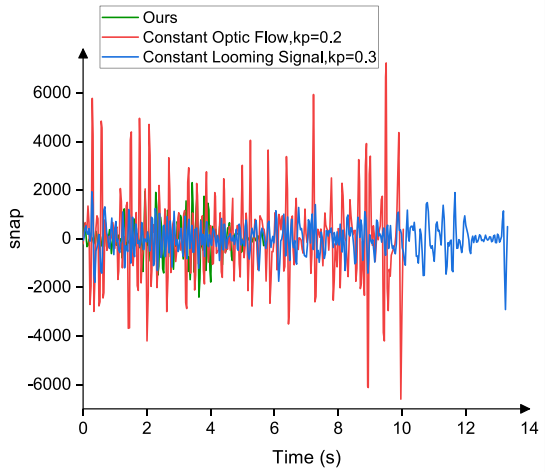

Figure 7. The fourth-order derivative of the descent trajectory with respect to time.

of the UAV shows less smoothness, which is reflected in figure 7, the landing based on optical flow is more noisy locally.

To comprehensively evaluate the performance of our proposed landing strategy, this study employed two key metrics for quantitative analysis, with the initial focus on the smoothness of the landing process. To this end, we introduced the concept of impulse as the criterion for the smoothness of the landing:

$$F \cdot \Delta t = 0 - mv_0. \tag{11}$$

In the formula, F represents the average force exerted (The net upward force of the UAV), Δt is the considered time interval, m is the mass of the drone, and v_0 is the initial velocity at the start of the impulse calculation. The meaning of this formula is to calculate the residual impulse of the UAV in the process of landing from a certain altitude to zero speed on the ground. The smaller the value of the impulse, the smaller the impact force suffered by the UAV when landing on the ground, and the smaller the braking force required to reduce its speed to zero. This method effectively quantifies the smoothness and safety of the drone's landing. We used a distance of 5 centimeters from the ground as the reference for the landing approach to calculate the remaining impulse of the drone under the control of various landing algorithms. The results are averaged over multiple measurements as shown in table 2.

Given that all experiments utilized the same drone, we uniformly set its mass parameter to 1. This setting does not compromise the assessment's validity. The smaller the impulse value, the less impact force on the drone. We hope that this value is as small as possible, as this will provide better protection for the drone equipment. Results demonstrate that under identical conditions, our landing strategy outperforms other methods in terms of stability and minimizes impact at landing. This is especially critical for missions involving sensitive instruments, as it ensures enhanced protection for the equipment carried by the drone.

Table 2. Landing smoothness index of each autonomous landing algorithm. The results of the impulse in the table are calculated for setting the drone mass to 1. If the mass is not set to 1, the unit of impulse is '$N \cdot s$'.

Autonomous landing algorithm	Impulse
Ours	0.111
Constant optical flow divergence strategy	0.312
The constant looming signal strategy	0.252

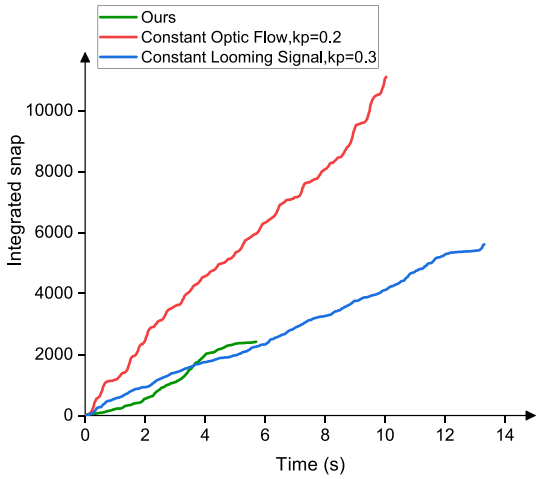

Figure 8. The absolute area of a snap curve is the enclosed area between the curve and the X-axis. The curve shown in the figure is the snap curve under the control of each autonomous control algorithm, which represents the growth trend of the cumulative energy consumption of the UAV during the landing process.

Next, we evaluated the flight efficiency throughout the landing process. In this context, we introduced the concept of snap, which is the fourth derivative of the motion trajectory with respect to time, used as a measure of flight efficiency. According to the literature [36, 37], a lower snap value indicates that the UAV can fly in a smoother manner. This not only reduces the mechanical stress on the UAV during landing but also effectively decreases energy consumption. Therefore, we used the snap curve as a metric to assess the performance of our designed landing method in practical applications. Figure 7 illustrates the fourth derivative of the autonomous landing trajectory under algorithmic control. To facilitate easier viewing of this metric, we calculated the absolute area under the snap curve within its domain (as shown in figure 8). It was evident that our landing strategy maintains higher efficiency throughout the flight, both overall and per unit time.

In terms of time efficiency, the optical flow strategy appears to be more advantageous in the early stage of landing (the first 3 s). However, embodied in energy efficiency is not necessarily the same result.

Since the optical flow in the field of view always deviates from the desired optical flow, the UAV needs to constantly adjust its speed, which leads to frequent changes in the mechanical stress of the UAV. This frequent change will show higher energy consumption in the snap curve. In contrast, our method uses less discrete output and increases the time delay; the frequency of speed adjustment is low, and the mechanical stress changes infrequently, so it shows better energy efficiency. The energy consumption can be calculated directly by measuring the battery consumption, but it is difficult to reveal some details of the landing process from the battery consumption process. By examining the snap curve, we can indirectly assess the level of UAV energy consumption, the smoothness of the flight trajectory, and how the mechanical stress changes. In fact, the battery consumption is not only related to the flight state, but also affected by external factors such as ambient temperature and humidity. Snap curve analyzes energy efficiency from the perspective of flight state, and although it cannot fully cover the impact of environmental factors, it can still be used as an effective reference index to evaluate energy efficiency and energy consumption.

4. Discussion

The looming-based landing strategy for UAVs has not yet been effectively implemented, possibly due to the fact that the biological mechanisms in nature that rely on looming cues for landing are not fully understood [22–24]. Additionally, traditional radar-based ranging methods have already been proven reliable for large aerial vehicle, while looming-based landing strategies face challenges in verification and trust. This paper presents a novel looming-based landing method for vertically capable flying robots. The proposed approach may not only offer insights into the understanding of biological systems that rely on looming cues for landing but also provide indirect applications for both practical use and the study of natural landing mechanisms. The proposed method has been validated in a simulation environment, demonstrating good performance across various landing surfaces. Although tests in sloped or dynamic scenarios have not yet been conducted, we remain confident in its capabilities. We compared our approach with an optical flow-based landing strategy. In terms of time efficiency, the optical flow strategy was faster during the initial phase of descent, whereas our method exhibited greater speed in the later stages of landing and showed no oscillations when approaching the ground.

In the experiments, although the overall landing performance was satisfactory, we also observed a certain degree of discontinuity in the landing speed. To fully leverage the potential of the looming-based strategy, several issues need further research and validation. We suspect that the primary cause of this discontinuity is the discrete output of the fuzzy controller, as the discreteness of the speed gain factors leads to irregular changes in velocity. Additionally, the irregularity of the LGMD signal and control delays may also contribute to this issue. By refining the output of the fuzzy controller, it may be possible to reduce or eliminate these discontinuities. It is necessary to further validate the robustness of the algorithm against environmental factors such as wind and lighting. In future work, more efforts should be involved to validate the algorithm in real world flight, and further enhance its adaptability and robustness.

5. Conclusions

This study introduces a landing strategy based on looming cues, successfully implementing autonomous landings in complex scenarios using fuzzy control technology. Simulation experimental results indicate that, compared to traditional constant optical flow divergence landing strategies, the method proposed in this study significantly enhances landing efficiency while ensuring stability and safety. Notably, our strategy prevents oscillation phenomena in the final phase of landing. Furthermore, we propose a mechanism to trigger the final landing, which not only provides an effective means for the drone's smooth landing but also offers valuable insights into the understanding of biologically inspired landing mechanisms.

Data availability statement

All data that support the findings of this study are included within the article (and any supplementary files).

Acknowledgments

I would like to thank Professor Zhao for his help in revising the manuscript of this paper. I would also like to thank the other authors for their valuable comments on this paper.

Conflict of interest

The authors declare that no competing interests exist.

ORCID iDs

Yupeng Xie https://orcid.org/0009-0004-0098-8394
Jiannan Zhao https://orcid.org/0000-0003-0052-3365

References

[1] Park S and Choi Y 2020 Applications of unmanned aerial vehicles in mining from exploration to reclamation: a review *Minerals* **10** 663

[2] Li X, Li Z, Wang H and Li W 2021 Unmanned aerial vehicle for transmission line inspection: status, standardization and perspectives *Front. Energy Res.* **9** 713634

[3] Talha M, Asghar F, Rohan A, Rabah M and Kim S H 2019 Fuzzy logic-based robust and autonomous safe landing for UAV quadcopter *Arab. J. Sci. Eng.* **44** 2627–39

[4] Bogue R 2010 Recent developments in miniature flying robots *Ind. Robot.* **37** 17–22

[5] Chahl J S, Srinivasan M V and Zhang S-W 2004 Landing strategies in honeybees and applications to uninhabited airborne vehicles *Int. J. Robot. Res.* **23** 101–10

[6] Srinivasan M V, Zhang S and Chahl J S 2001 Landing strategies in honeybees and possible applications to autonomous airborne vehicles *Biol. Bull.* **200** 216–21

[7] Goyal P, Baird E, Srinivasan M V and Muijres F T 2023 Visual guidance of honeybees approaching a vertical landing surface *J. Exp. Biol.* **226** jeb245956

[8] Lee D N, Davies M N, Green P R and Van Der Weel F 1993 Visual control of velocity of approach by pigeons when landing *J. Exp. Biol.* **180** 85–104

[9] Lee D N, Reddish P E and Rand D 1991 Aerial docking by hummingbirds *Naturwissenschaften* **78** 526–7

[10] Whitehead J G, Worrell T and Socha J J 2023 Mallard landing behavior on water follows a-constant braking strategy *J. Exp. Biol.* **226** jeb244256

[11] Phan H V and Park H C 2020 Mimicking nature's flyers: a review of insect-inspired flying robots *Curr. Opin. Insect Sci.* **42** 70–75

[12] Floreano D, Zufferey J-C, Srinivasan M V and Ellington C 2009 *Flying Insects and Robots* (Springer)

[13] Lentink D 2014 Bioinspired flight control *Bioinspiration Biomim.* **9** 020301

[14] Collett T S 2002 Insect vision: controlling actions through optic flow *Curr. Biol.* **12** R615–7

[15] Van Breugel F, Morgansen K and Dickinson M H 2014 Monocular distance estimation from optic flow during active landing maneuvers *Bioinspir. Biomim.* **9** 025002

[16] de Croon G C 2016 Monocular distance estimation with optical flow maneuvers and efference copies: a stability-based strategy *Bioinspir. Biomim.* **11** 016004

[17] Ho H W, de Croon G C and Chu Q 2017 Distance and velocity estimation using optical flow from a monocular camera *Int. J. Micro Air Veh.* **9** 198–208

[18] Ho H W, de Croon G C, Van Kampen E, Chu Q and Mulder M 2018 Adaptive gain control strategy for constant optical flow divergence landing *IEEE Trans. Robot.* **34** 508–16

[19] de Croon G C, De Wagter C and Seidl T 2021 Enhancing optical-flow-based control by learning visual appearance cues for flying robots *Nat. Mach. Intell.* **3** 33–41

[20] Kendoul F 2014 Four-dimensional guidance and control of movement using time-to-contact: application to automated docking and landing of unmanned rotorcraft systems *Int. J. Robot. Res.* **33** 237–67

[21] Baird E, Boeddeker N, Ibbotson M R and Srinivasan M V 2013 A universal strategy for visually guided landing *Proc. Natl Acad. Sci.* vol **110** 18686–91

[22] Egelhaaf M 2023 Optic flow based spatial vision in insects *J. Comp. Physiol.* A **209** 541–61

[23] Mauss A S and Borst A 2020 Optic flow-based course control in insects *Curr. Opin. Neurobiol.* **60** 21–27

[24] Ache J M, Namiki S, Lee A, Branson K and Card G M 2019 State-dependent decoupling of sensory and motor circuits underlies behavioral flexibility in drosophila *Nat. Neurosci.* **22** 1132–9

[25] Zhao J, Wang H, Bellotto N, Hu C, Peng J and Yue S 2021 Enhancing lgmd's looming selectivity for uav with spatial–temporal distributed presynaptic connections *IEEE Trans. Neural Netw. Learn. Syst.* **34** 2539–53

[26] Sztarker J and Rind F C 2014 A look into the cockpit of the developing locust: looming detectors and predator avoidance *Dev. Neurobiol.* **74** 1078–95

[27] Rind F C, Wernitznig S, Pölt P, Zankel A, Gütl D, Sztarker J and Leitinger G 2016 Two identified looming detectors in the locust: ubiquitous lateral connections among their inputs contribute to selective responses to looming objects *Sci. Rep.* **6** 35525

[28] Rind F C and Bramwell D 1996 Neural network based on the input organization of an identified neuron signaling impending collision *J. Neurophysiol.* **75** 967–85

[29] Blanchard M, Rind F C and Verschure P F 2000 Collision avoidance using a model of the locust lgmd neuron *Robot. Auton. Syst.* **30** 17–38

[30] Yue S, Rind F C, Keil M S, Cuadri J and Stafford R 2006 A bio-inspired visual collision detection mechanism for cars: optimisation of a model of a locust neuron to a novel environment *Neurocomputing* **69** 1591–8

[31] Stafford R, Santer R D and Rind F C 2007 A bio-inspired visual collision detection mechanism for cars: combining insect inspired neurons to create a robust system *BioSystems* **87** 164–71

[32] Silva A, Silva J B and Santos C 2012 *LGMD Based Neural Network for Automatic Collision Detection* (SCITEPRESS)

[33] Krejan A and Trost A 2011 Lgmd-based bio-inspired algorithm for detecting risk of collision of a road vehicle *2011 7th Int. Symp. on Image and Signal Processing and Analysis (ISPA)* (IEEE) pp 319–24

[34] Symeonidis C and Nikolaidis N 2022 Simulation environments *Deep Learning for Robot Perception and Cognition* (Elsevier) pp 461–90

[35] Ma C, Zhou Y and Li Z 2020 A new simulation environment based on airsim, ROS, and PX4 for quadcopter aircrafts *2020 6th Int Conf. on Control, Automation and Robotics (ICCAR)* (IEEE) pp 486–90

[36] Mellinger D and Kumar V 2011 Minimum snap trajectory generation and control for quadrotors *2011 IEEE Int Conf. on Robotics and Automation* (IEEE) pp 2520–5

[37] Kreciglowa N, Karydis K and Kumar V 2017 Energy efficiency of trajectory generation methods for stop-and-go aerial robot navigation *2017 Int. Conf. on Unmanned Aircraft Systems (ICUAS)* (IEEE) pp 656–62